Calcif Tissue Int (1995) 56:297–304

Calcified
Tissue
International

Scanning Electron Microscopy and Molecular Modeling of Inhibition of Calcium Oxalate Monohydrate Crystal Growth by Citrate and Phosphocitrate

A. Wierzbicki,[1] C. S. Sikes,[2] J. D. Sallis,[3] J. D. Madura,[1] E. D. Stevens,[4] K. L. Martin[4]

[1]Department of Chemistry, University of South Alabama, Mobile, Alabama 36688
[2]Department of Biological Sciences, University of South Alabama, Mobile, Alabama 36688
[3]Department of Biochemistry, University of Tasmania, Hobart, Tasmania 7001, Australia
[4]Department of Chemistry, University of New Orleans, New Orleans, Louisiana 70148

Received: 9 August 1994 / Accepted: 13 September 1994

Abstract. Binding of citrate and phosphocitrate to calcium oxalate monohydrate crystals has been studied using scanning electron microscopy (SEM) and molecular modeling. Phosphocitrate structure has been resolved using low temperature X-ray analysis and *ab initio* computational methods. The (−1 0 1) crystal surface of calcium oxalate monohydrate is involved in binding of citrate and phosphocitrate, as shown by SEM and molecular modeling. Citrate and phosphocitrate conformations and binding energies to (−1 0 1) faces have been obtained and compared to binding to another set of calcium-rich planes (0 1 0). Difference in inhibitory properties of these compounds has been attributed to better coordination of functional groups of phosphocitrate with calcium ions in (−1 0 1). Relevance of this study to design of new calcium oxalate monohydrate inhibitors is discussed.

Key words: Calcium oxalate monohydrate — Inhibition — Citrate and phosphocitrate binding — X-ray structure of phosphocitrate — Molecular modeling.

Citrate and phosphocitrate (PC) are both recognized to be strong inhibitors of the nucleation, growth and aggregation of calcium oxalate monohydrate (COM) crystals [1–3]. COM is widespread in organisms where it serves a number of functions. For example, in plants it is a useful metabolite and structural component [4, 5] and in marine organisms, it is found in the main sediment-forming organisms of the oceans, echinoderms, and mollusks [6]. In man, the formation of this calcium salt is undesirable as it leads to the development of obstructive calculi in the kidney and urinary tract. Information on inhibitor-crystal surface interactions is important toward the development of potent stereospecific compounds to control, and if possible, to eliminate the crystallization and aggregation of this calcium salt.

Molecular modeling together with electron microscopy of the habits of crystals grown in the presence of these inhibitors can be used to elucidate the stereospecificity of action of known inhibitors and to design more efficient inhibitors. Scanning electron microscopy (SEM) provides information on crystal morphology changes induced by interactions with adsorbate molecules. Expression of specific faces of the crystals indicates possible interactions between the inhibitor and the atomic pattern of those particular crystal surfaces. Such interactions are very often based upon the stereospecificity of inhibitor-surface recognition. Molecular modeling can provide valuable insight into energetic and spatial feasibility of such recognition.

Recently, for example, we have documented the changes in calcium carbonate crystallization in marine organisms in the presence of matrix proteins [7]. Of particular interest was an almost perfect match between polyaspartates found in β sheet conformation in the natural polypeptides and the specific prism faces (1 −1 0) along the c axis of the calcite crystal. The nature of this match appears to be based on the ability of the carboxylate groups of the $(Asp)_n$ inhibitor to complete the calcium ion coordination polyhedra disrupted at the surface due to crystal bulk termination. Important features of surface (1 −1 0) are perpendicularity and spacing of carbonate ions that afford optimal binding of incoming carboxylate groups of the inhibitor. Reports on interactions between acidic matrix macromolecules and calcite [8] and calcium phosphate ester crystals [9], interactions between dicarboxylates and calcite [10], and also aragonite (Wierzbicki and Sikes, in preparation) confirms that this mechanism of crystal inhibition based on stereospecificity of interaction is more general and extends to broader classes of crystal forms. Similar conclusions have been reached with respect to barium sulfate inhibition by phosphonates [11].

If the same principles are applied to the binding of the citrate or PC molecules, both compounds should interact stereospecifically with certain planes of COM. Among possible crystal surfaces, (−1 0 1) planes contain loci of calcium ions that seem to be perfectly suited for inhibitor binding leading to stabilization of these faces and the slowing of the growth in the direction perpendicular to them [12]. Moreover, citrate-based inhibitors bound to (−1 0 1) planes encounter oxalate groups perpendicular to (−1 0 1) that create an excellent binding environment for carboxylate groups of the inhibitor which would complete the coordination polyhedra of calcium cations. This binding scheme is much akin to the calcium carbonate crystal inhibition described above. Of interest, plane (−1 0 1) of COM also has been identified as the potential binding plane for nephrocalcin, an acidic macromolecule contained in mammalian urine [13].

The present studies report on the results of binding of citrate and phosphocitrate to the calcium-rich surfaces of COM crystals. Molecular modeling of binding and SEM of crystals grown in the presence of the two compounds were

Correspondence to: C. S. Sikes

Table 1. Characterization of calcium oxalate monohydrate surfaces used for analysis of interactions with citrate and phosphocitrate

	Surface			
	(−1 0 1)		(0 1 0)	
Angle (U,V)	90°		107.05°	
Vector U	[1 0 1]		[0 0 1]	
Vector V	[0 1 0]		[1 0 0]	
Length U	10.114		6.319	
Length V	14.588		9.976	
Size	[4U 3V]		[7U 5V]	
	Complete	Incomplete	Complete	Incomplete
Number of atoms	1920	1914	2100	2094
Depth	12.0	12.0	12.0	12.0
Citrate binding Energy	−546	−1071	−108	−502
Phosphocitrate (αβ) Binding energy	−717	−1424	−142	−675
Phosphocitrate (αα) Binding energy	−699	−1346	−167	−622

Surface unit mesh vectors are defined as U and V. Lengths are reported in Angstroms and binding energies in kcal/mol. Incomplete surface designates the surface with one oxalate group removed

used to explain the inhibitory properties of these molecules and also to account for the observed differences in their inhibitory activity.

Materials and Methods

SEM Studies of Crystal Growth

The method of Sutor [14] modified as described by Sallis and Lumley [15] was used as the source of crystal material. Solutions of 0.1 M $CaCl_2$ and 0.1 M NaOx were allowed to diffuse down filter paper wicks into a buffered solution of 0.2 M sodium acetate (pH 6.1) in the presence or absence of inhibitor. Growth of COM was initiated by immersing glass fibers into the reaction solution. After 20 hours, the fibers were lifted clear of the reacting solution, allowed to air dry, and then mounted on stubs for SEM (Phillips SEM 505). PC was prepared as the sodium salt by phosphorylation of tribenzyl citrate followed by deprotection through hydrogenation [16]. The monosodium salt was crystallized from water and then subsequently brought to pH 7.0 with additional alkali. Sodium citrate was purchased from Sigma-Aldrich, Australia.

Modeling Procedure of Citrate and PC Interactions with COM

The computational procedure developed for calcium carbonate inhibition by polyaspartate [7] and ice inhibition by antifreeze proteins [17] was used to investigate the stereospecificity of the calcium oxalate inhibitors. Calcium oxalate crystal data are available from the literature [12, 18] and for the purpose of modeling, the structure proposed by Deganello and Piro [12] for investigation of the interaction between COM and nephrocalcin [13] was applied. In this structure, COM crystallizes in the monoclinic space group $P2_1/n$ with a = 9.9763 Å, b = 14.5884 Å, c = 6.2913 Å, β = 107.05°, and Z = 8. A CERIUS (Molecular Simulations, Inc., Burlington, MA) materials sciences modeling package enabled the generation of the COM crystal structure from fractional coordinates listed in [12] along with unit cell and symmetry data. As hydrogen atom positions for the water molecules were not previously resolved [12], CERIUS was used to build hydrogen atoms onto the water oxygen, and the hydrogen positions in the lattice were obtained by applying short-term dynamics followed by minimization procedures. Consideration of the COM crystal structure showed that COM crystals contain two sets of crystallographically nonequivalent oxalate groups which results in two distinct types of essentially planar packing. One is within (−1 0 1) crystal planes and the other interlocks the (−1 0 1) along the c axis, being almost perpendicular to it. The structure is additionally stabilized by a network of hydrogen bonding involving water molecules. Plane (−1 0 1) is characterized by a high density of calcium ions. Another calcium-rich plane is the (0 1 0) plane of COM, containing approximately 18.3% less calcium cations per unit area than (−1 0 1). Using CERIUS, (−1 0 1) and (0 1 0) surfaces of COM were prepared according to specifications listed in Table 1.

Structural and Electrostatic Parameter Determinations for Citrate and PC Using Computational Methods

The geometric structure of citrate was obtained using a series of geometry optimizations for a neutral citrate molecule applying both *ab initio* and semiempirical methods. The citrate structure, but not the PC molecule structure, has been characterized previously by x-ray analysis [19]. Geometry optimization of citrate revealed a structure consistent with the x-ray geometry, with a planar backbone and central carboxyl and hydroxyl group lying in the plane perpendicular to the backbone. The hydrogen of the hydroxyl group is within the hydrogen bond distance to oxygen of the central carboxyl. Citrate, when present in urine, is subject to a pH range between 6 and 8 which would result in deprotonation of all the carboxyl groups. Therefore, to determine the electrostatic charge distribution for the citrate three-valent anion, a single point calculation was run to fit charges from electrostatic potentials [20, 21]. This method of charge determination has proven to determine reliable atomic charges, in fact better than those derived from Mulliken population analysis. Both geometry optimization and charge determination were performed using Spartan (Wavefunction, Inc., Irvine, CA), an electronic structure computational program. Geometric and electrostatic parameters determined in this manner were incorporated into a CHARMm (Molecular Simulations, Inc., Burlington, MA) parameters file and used at later stages of modeling for optimizing citrate-COM surface interactions.

Geometry optimizations for PC were derived from the semiempirical method, Modified Neglect of Differential Overlap (MNDO,

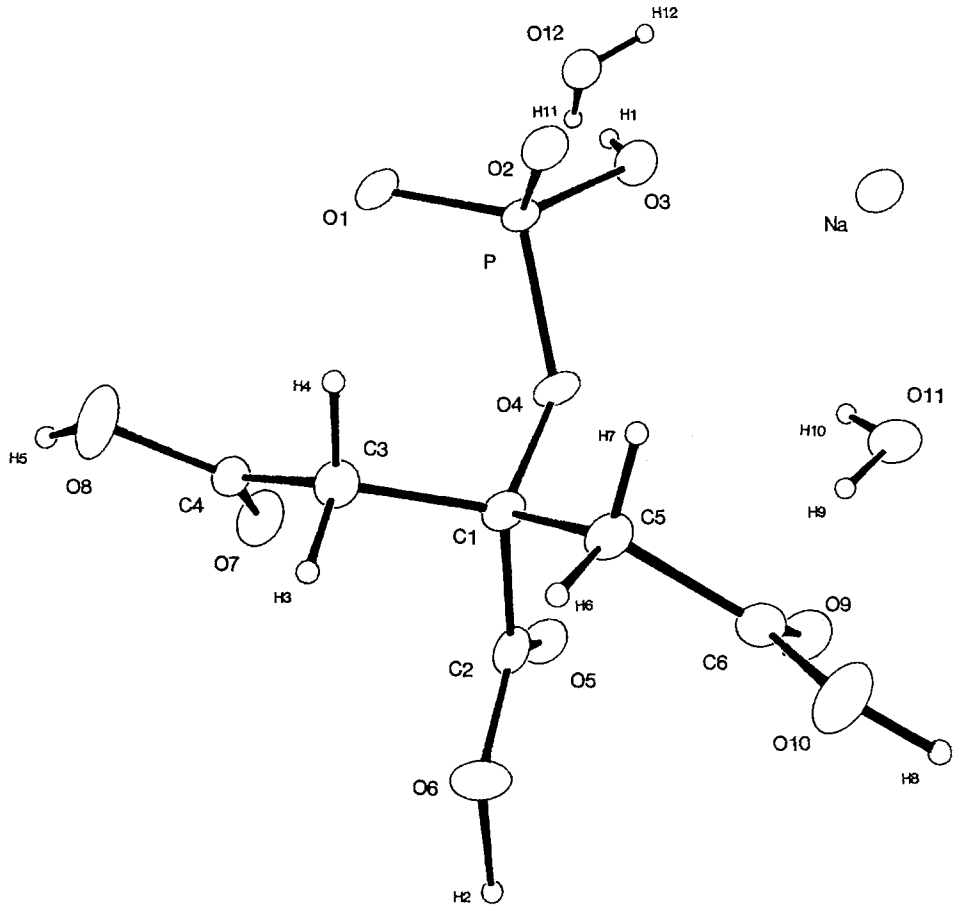

Fig. 1. Asymmetric unit of monosodium phosphocitrate dihydrate crystal as revealed by low temperature x-ray crystallography. The x-ray structure of PC was used, along with the computationally determined geometry, for modeling of interaction of PC with COM crystals.

Spartan), and *ab initio* Hartree-Fock (Gaussian 92, Gaussian Inc., Pittsburgh, PA), using 6-31G** basis set, and indicated a planar backbone and co-planarity of central carboxyl group with PO_4 group symmetry plane. In the MNDO method, certain integrals were taken as zero or derived from spectroscopic measurements [22, 23]. The Hartree-Fock method is based on the replacement of the full many-electron wave function by a single determinant of products of one-electron functions. The notation, 6-31G**, refers to a split-valence set with polarization and with the addition of p-functions to each hydrogen, which provides the best *ab initio* results for large, second-row-element molecules [24].

Because in the pH range 6–8, groups from one of the P-OH, a central COOH (β), one outer COOH (α), and as the more alkaline value is obtained, the second P-OH are deprotonated, single point calculations were run to determine the electrostatic charges from the electrostatic potential for a four-valent anion of PC. We call this deprotonation sequence (α,β). Geometrical parameters for the oxalate anion were developed in a similar way using *ab initio* Hartree-Fock calculations with 6-31G** basis set, and the charges were determined from electrostatic potentials as above. To confirm the geometry of PC, as obtained by computational methods, we performed low temperature x-ray analysis of the crystals of monosodium phosphocitrate dihydrate.

X-ray Determination of PC Structure

The crystal structure of monosodium phosphocitrate dihydrate has been determined by single-crystal x-ray diffraction methods at low temperature [25]. A colorless plate with approximate dimensions 0.3 × 0.2 × 0.1 mm was selected for data collection and mounted on an Enraf-Nonius CAD4 x-ray diffractometer. The crystal was cooled to 105(2)K in a stream of N_2 gas and the temperature was monitored using a copper-constantan thermocouple. The cell dimensions were determined by least-squares refinement of the setting angles of 25 reflections with 30°2θ50° using MoKα radiation. Unit cell dimensions and systematic absences 0k0: k = 2n + 1 and h0*l*:*l* = 2n + 1 indicated the monoclinic space group $P2_1/c$ with a = 12.385 Å, b = 7.007 Å, c = 14.889 Å, and β = 109.02° and number of molecules per cell Z = 4. X-ray intensities were measured using ω = 2θ scans within the ranges $4 \leq 2\theta \leq 54°$, $0 \leq h \leq 15$, $0 \leq k \leq 8$, $-18 \leq l \leq 18$. Three standard intensities, measured at 2-hour intervals, showed a decline of less than 0.5% during data collection. Absorption as a function of rotation around the scattering vector (ψ) was measured and an empirical correction applied, with relative transmission coefficients ranging from 0.817 to 0.996. Lorentz and polarization corrections were applied to a total of 3184 reflection intensity measurements. Averaging of symmetry-related reflections yielded 2632 independent reflections with an internal agreement of 4.1%, of which 1568 were considered observed [$I > 3\sigma(I)$, where σ(I) is the estimated standard deviation in the net intensity].

The structure was determined by the direct methods using MULTAN80 [26]. Peaks corresponding to the 20 non-H atoms were located in a map calculated by Fourier summation of nesonalized structure factors and the positions of the 12 H atoms were located in subsequent Fourier summations. Refinement was by full-matrix least-squares minimization of $\Sigma w(|F_o|-|F_c|)^2$, where $w = 1/\sigma^2(F)$ and $\sigma^2(F^2) = \sigma_{cs}{}^2 + (0.04F^2)^2$. Positions and anisotropic thermal parameters were refined for non-H atoms, positions and isotropic thermal parameters for H atoms. The final agreement factors were R = 4.2%, R_w = 5.3%, and S = 1.91 for 229 variables. Atomic scattering factors and anomalous dispersion corrections were taken from the International Tables for X-ray Crystallography [27] and all computer programs used were from the SDP system [28]. An asymmetric unit of monosodium phosphocitrate dihydrate is shown in Figure 1.

X-ray analysis of PC structure was performed after *ab initio* computational determination of PC geometry was done yielding al-

most exactly the same bond lengths and bond angles. The only discrepancy between the *ab initio* structure of PC and the x-ray structure was that the x-ray structure revealed a slightly nonplanar backbone chain, and PO_4 group symmetry plane was not coplanar with the central carboxylate group of PC yielding C2-C1-04-P dihedral angle 156.2° with additional torsion about 04-P bond (Fig. 1). The calculated bond lengths and angles were in excellent agreement with the x-ray data, with only the above-mentioned dihedral angles showing some discrepancy. This discrepancy is not unexpected due to usually low potential barriers for the dihedral angles. The dihedral angle modification observed in the crystal form of PC anion is due to intermolecular interactions within the crystal, especially hydrogen bonds and electrostatic interactions with the sodium ion, that lead to optimal packing, not necessarily corresponding to optimal energy of isolated molecule. Detailed comparison of the computational and x-ray structures of PC is presented elsewhere (Wierzbicki and Stevens, in preparation).

Inhibitor-Surface Energy Optimization Procedure

Using QUANTA (Molecular Simulations, Inc., Burlington, MA) molecular modeling software, the inhibitor molecule in the initial conformation was positioned near the COM surface within the electrostatic interaction range and the CHARMm energy optimization procedure was applied. Computationally determined geometrical and electrostatic parameters for the COM surface and for the inhibitors were incorporated into CHARMm parameters file. The minimization procedure takes into account the contributions from electrostatic forces, van der Waals forces, hydrogen bonds, bonds, angles, and dihedral angles to the total energy of the system. Starting from the initial position of citrate/PC-surface system, the total energy was minimized yielding the energy and geometry of the most favorable position of citrate/PC on the crystal surface. During minimization, the coordinates of crystal lattice atoms were kept fixed and the inhibitor molecule was allowed to translate, rotate, and adopt any conformation on the COM surface. The binding energy was determined as the difference between the energy of the citrate/PC-COM system and the sum of the citrate/PC and COM energies when separated beyond the interaction distance.

Two possible scenarios for interaction between the citrate/PC and the COM surface were considered, namely, that the inhibitor molecule interacts with the complete surface of COM or that the inhibitor interacts with the COM surface in which one oxalate group is removed. This approach allows an anionic group of the inhibitor molecule to substitute for the oxalate anion's lattice position at the surface. The effect of solvent was analyzed by introducing an 8 Å hydration shell around the inhibitor molecule and repeating the minimization procedure. The final configuration of the system was the same as the electrostatic interactions between the COM surface and the inhibitor was the driving force determining the final geometry of the system. The water molecules were accommodated around the inhibitor slightly modifying the attraction of the molecule to the surface but having no effect on mechanism of binding to the surface. For this reason, further consideration was given to the inhibitor surface system only, using a constant dielectric model with dielectric constant equal to one.

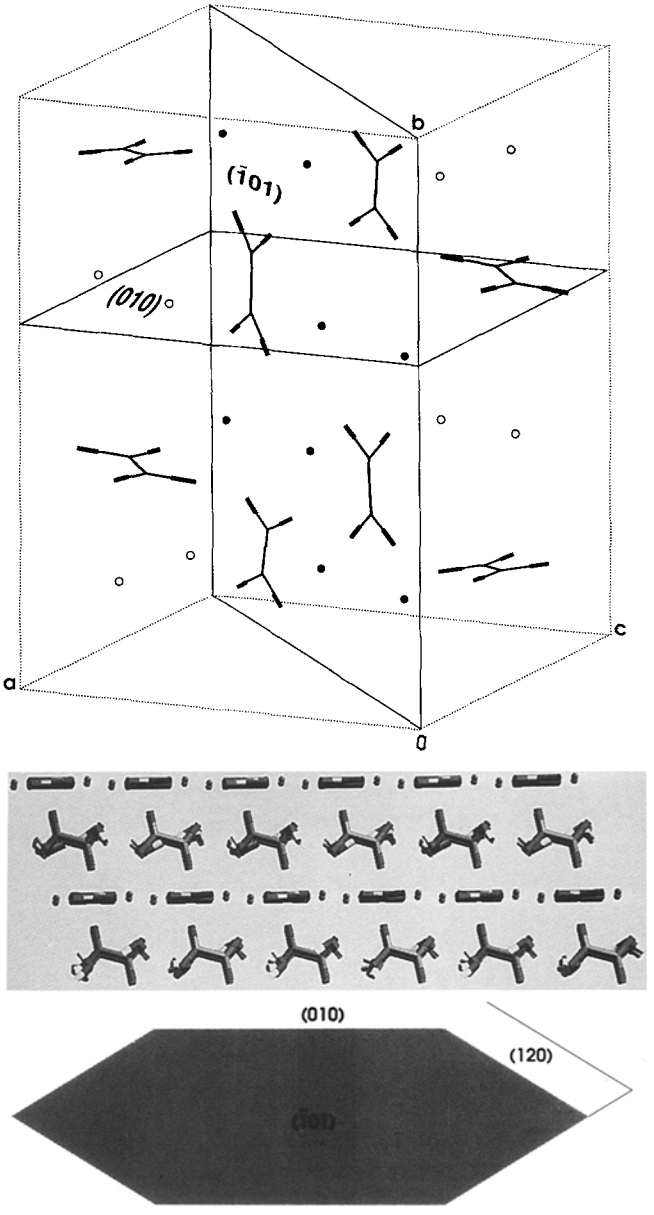

Fig. 2. Computer models of COM. **(A)** Unit cell of COM, as determined in [13]: a-axis (0a), b-axis (0b), c-axis (0c). Crystal faces analyzed for interaction with citrate and phosphocitrate are indicated with heavy lines. Solid circles represent calcium atom positions and open circles indicate positions of water oxygens. **(B)** Side view of a COM surface slab, used for modeling purposes, facing (0 1 0) plane. Shown are two (−1 0 1) planes perpendicular to the plane of the picture. **(C)** COM crystal morphology.

Results

Figure 2A shows the unit cell of COM. Computer-drawn COM crystal morphology depicting (−1 0 1) and (0 1 0) faces is shown in Figure 2C. Figure 2B shows the side view of the COM crystal slab used for the modeling. Although the planes (1 1 0) were identified as of higher probability growth faces than (1 2 0), Figure 2C shows (1 2 0) faces that have an apex angle almost identical to the fast-growing apical planes seen in Figure 3. Control crystals of COM are shown in Figure 3 with clearly expressed (−1 0 1) and (0 1 0) faces. Some crystals show evidence of twinning along (−1 0 1) as seen in Figure 3B.

SEMs of COM crystals grown in the presence of citrate (Fig. 4) and PC (Fig. 5) revealed stabilized (−1 0 1) faces. An increase in nonspecific morphological effects of PC was observed at higher doses (Fig. 6). Molecular models of the adsorbates with both complete and incomplete (−1 0 1) surfaces are shown in Figures 7–10.

Discussion

When the crystals were grown subject to interaction with citrate and PC, plane (−1 0 1) was clearly stabilized at the

Fig. 3. SEM of COM. **(A)** Crystals grown in the absence of the inhibitor showing clearly expressed (−1 0 1) faces, bar = 0.1 mm. **(B)** Crystals grown in the absence of the inhibitor showing twinning along (−1 0 1) faces, bar = 0.1 mm.

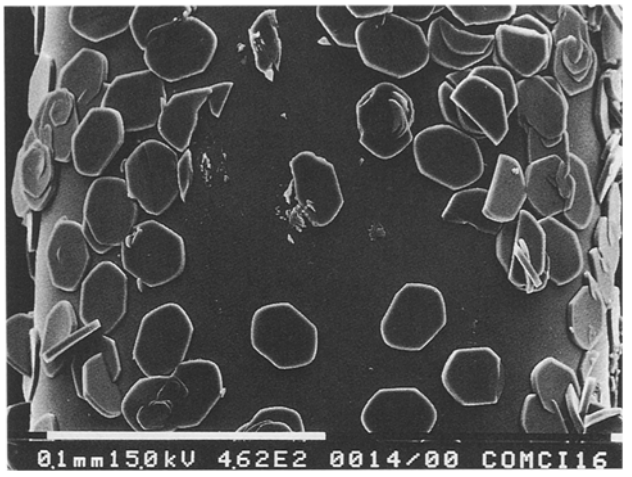

Fig. 4. SEMs of COM crystals grown in the presence of initial amount of 1.3 mg/ml of citrate. The faces (−1 0 1) were enlarged relative to the other faces, the length to width ratio was significantly decreased, and the crystals were smaller when compared with controls, bar = 0.1 mm.

expense of the other faces indicating preference for interaction with the atomic motif of this surface for both inhibitors. In the presence of citrate, the faces (−1 0 1) were enlarged and the length-to-width ratio was significantly decreased. There was only slight rounding of the crystal angles suggesting stereospecific interaction with (−1 0 1) plane (Fig. 4). The effect of PC is even more dramatic. At a low concentration (0.05 mg/ml), apical planes were not present at all and (−1 0 1) faces were well stabilized (Fig. 5A). The effect of PC at this initial concentration was similar to the effect observed for nephrocalcin [13]. In some instances, planes (−1 0 1) were stabilized, but additionally, the curvature of the edges of these faces was enhanced. Slightly curved, boat-shape crystals indicated that in addition to the specific interactions with (−1 0 1) faces, there were other, perhaps non-specific, interactions between the PC and the crystal (Fig. 5B). In comparison with citrate this could be attributed, among the other factors discussed below, to the higher ionic charge of PC under the conditions studied. This effect was intensified with the increased dosage of 0.25 mg/ml of PC, resulting in irregularly overgrown COM crystals indicating much less specific inhibition (Fig. 6). In general, dosages of PC about 20-fold lower than those of citrate were required to cause similar morphological changes. SEM images also revealed that PC causes significant diminishing of COM crystal size.

Molecular modeling of binding to the complete (−1 0 1) surface of COM revealed that the citrate molecule oriented itself on the surface in the position such that all of its carboxylate groups interacted with the calcium ions of the surface. This orientation allowed the carboxylate groups to partially complete calcium coordination polyhedra at the surface (Fig. 7). For clarity of presentation, only the top layer of the surface atoms is shown. The citrate molecule fits well to a trapezoidal arrangement of calcium ions between oxalate groups. Carboxylate groups of citrate were somewhat rotated when compared with an isolated citrate molecule, but overall, there was no major distortion of the molecular shape.

The stereospecificity of the interaction in this case was achieved due to excellent matching of the separation of carboxylate groups of citrate to the calcium ion distribution at the surface. The molecule was slightly shifted with respect to the calcium ion trapezoid due to the fact that hydrogen from the hydroxyl group interacted with one of oxalate oxygens. Citrate carboxylate groups approach the surface at the angle which would be the closest possible to perpendicular to the surface, just like incoming oxalate ions would if the crystal lattice was to be continued.

Binding of PC to the complete (−1 0 1) surface of COM followed a different pattern (Fig. 8). Because PC is bigger than citrate, it coordinated with six instead of four calcium ions. Binding energy, −717 kcal/mol, was significantly greater than the binding energy of citrate, −546 kcal/mol. In this case, the binding-site recognition occurred due to matching of the shape of PC with calcium ions in a hexagonal arrangement at the surface.

During COM crystal growth, inhibitor molecules may not only interact with complete (−1 0 1) surfaces but they are also likely to substitute for oxalate groups into the growing crystal lattice. To investigate the stereospecificity of citrate and PC substitution into the (−1 0 1) surface, one oxalate group was removed from the surface, and the energy minimization procedure was repeated for the inhibitor-surface system. The shape and the charge distribution of the inhib-

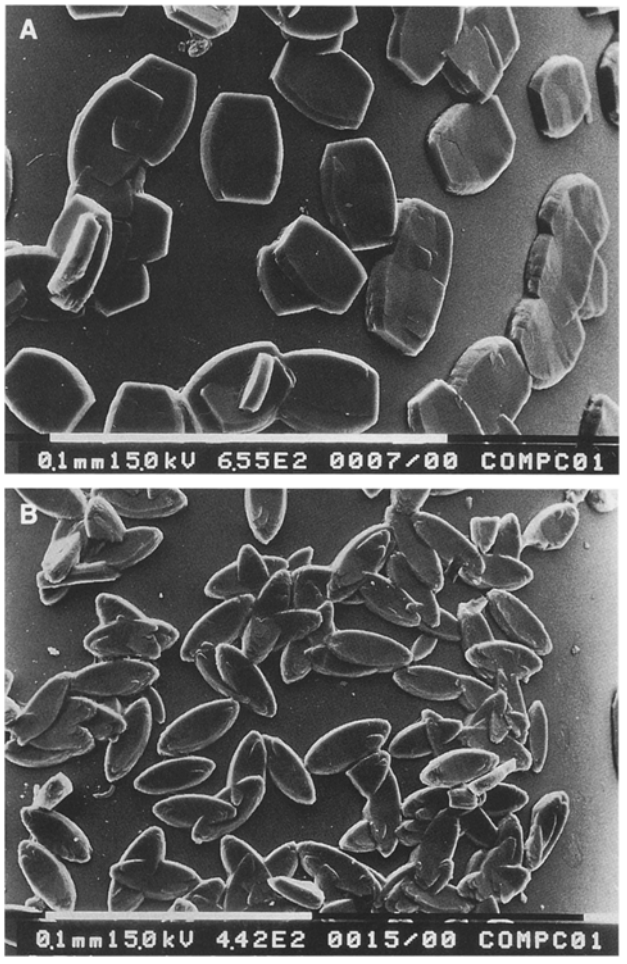

Fig. 5. The effect of PC on morphology of COM. **(A)** SEM image of crystals grown in the presence of initial amount of 0.05 mg/ml of PC. The (−1 0 1) faces were stabilized, and fast-growing apical planes were not present. Crystal morphology changes were similar to the ones induced by nephrocalcin [13]. **(B)** SEM image of crystals grown in the presence of initial amount of 0.05 mg/ml of phosphocitrate. Planes (−1 0 1) were stabilized and slightly-curved. Boat-shaped crystals suggested that, as crystal growth proceeded and the concentration of PC became depleted, there were less specific effects of PC on crystal morphology, bar = 0.1 mm.

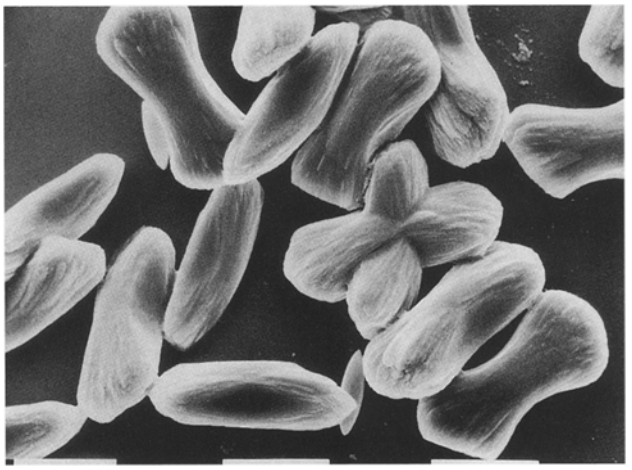

Fig. 6. SEM image of COM crystals grown in the presence of the initial amount of 0.25 mg/ml of PC. The morphology changes seen in Figure 5B were intensified and crystals were observed that were irregularly overgrown due to large concentration of the inhibitor, bar = 0.01 mm.

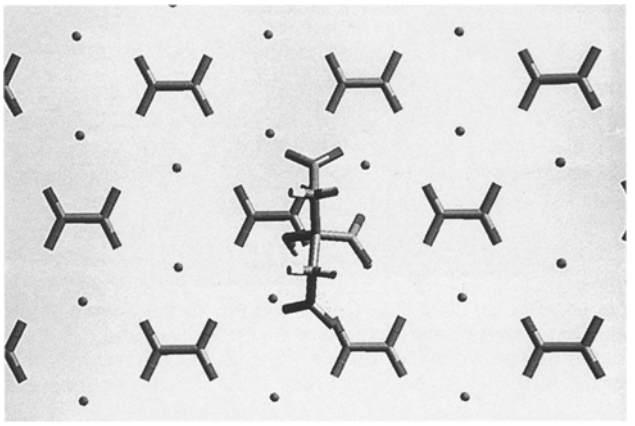

Fig. 7. Computer model of a citrate molecule interacting with complete (−1 0 1) surface of monohydrate. For clarity of presentation, top view of only one layer of the surface is shown. Citrate molecule is coordinated with four calcium ions. The molecule is slightly shifted due to citrate hydroxyl group interacting with oxalate oxygen.

itor is even more important here as the inhibitor must be able to fit into the space created by the oxalate ion removal and to coordinate with neighboring calcium ions. The citrate molecule clearly fit very well into the oxalate ion position with all three carboxylate groups involved in binding to the surface, with binding energy increased significantly to −1071 kcal/mol. All six negatively charged carboxylate groups' oxygens were less than 2.6 Å from the neighboring calcium ions (Fig. 9).

It was apparent that there is a possibility to improve binding of citrate-based inhibitors by replacing the hydroxyl group of citrate with a relatively small and negatively charged functional group, such as the PO_4 group of PC, to allow for a better coordination with calcium ions. The optimal binding geometry of PC to (−1 0 1) incomplete planes of COM involved the coordination of the phosphate group with four calcium ions (Fig. 10), with all of the oxygens of phosphate less than 2.7 Å away from the closest calcium ions. Moreover, the β carboxyl group was coordinated with three calcium ions and the binding energy was lowered to −1424 kcal/mol. Analysis of PC binding to the (−1 0 1) surface indicated high stereospecificity of inhibitor-substrate recognition and suggested why PC performs as a better inhibitor than citrate.

Citrate and PC binding to (0 1 0), another calcium-rich plane of COM, was also compared. Again, both complete and incomplete surfaces were considered (Table 1). For complete (0 1 0) surfaces, interactions of both citrate and PC were not stereospecific and the binding energies were much less favorable, i.e., −108 and −142 kcal/mol, respectively. The geometry of optimal binding revealed no inhibitor-surface recognition which instead was based on the overall attraction between rows of positively charged calcium ions and the negatively charged inhibitor molecule that was drawn to the surface. When considering the incomplete (0 1 0) surface, citrate can almost fit into the space created by oxalate ion removal. However, the calcium ion distribution

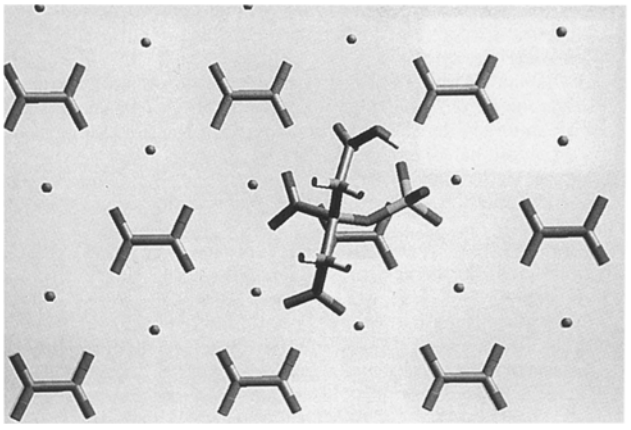

Fig. 8. Computer model of a PC molecule interacting with complete (−1 0 1) surface of COM. The molecule is coordinated with six calcium ions. The PO_4 group is slightly bent to minimize interaction with negative charge on the oxalate ion.

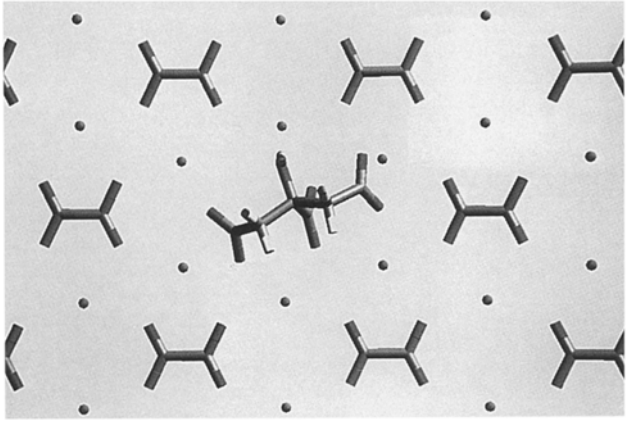

Fig. 9. Computer model of a citrate molecule interacting with incomplete (−1 0 1) surface of COM, view as in Figure 7. Hydroxyl hydrogen pointing away from the surface. The citrate molecule is now coordinated with six calcium ions. The molecule is somewhat rotated due to slight asymmetry of the crystal electrostatic field, as this structure was obtained using unrestricted energy minimization.

did not match the distribution of the functional groups of citrate. Binding of PC to the incomplete (0 1 0) surface was also nonspecific and based predominantly on electrostatic interaction between the surface cations and the PO_4 group that was drawn deep into the surface. Binding energies in this case were −675 kcal/mol and −502 kcal/mol for PC and citrate, respectively.

Until recently, the sequence of deprotonation in the PC molecule was believed to follow a different order than used in this paper. Namely, in the pH range 6–8, groups from one of the P-OH, two outer COOH (α,α), and, as the more alkaline value of pH was obtained, the second P-OH were believed to be deprotonated leaving a proton on the central COOH (β) group. Recent experimental data (Sallis, in preparation), however, indicate that the central COOH (β) group may be deprotonated leaving one of the α COOH protonated. In Table 1, the energy minimization results for (α,α) deprotonation are also given. Somewhat better binding of PC was predicted for the (α,β) deprotonation sequence. The energy gain was due to better coordination of β carboxylate with three surface calcium ions when compared with (α,α) binding where central carboxylate was not participating in binding.

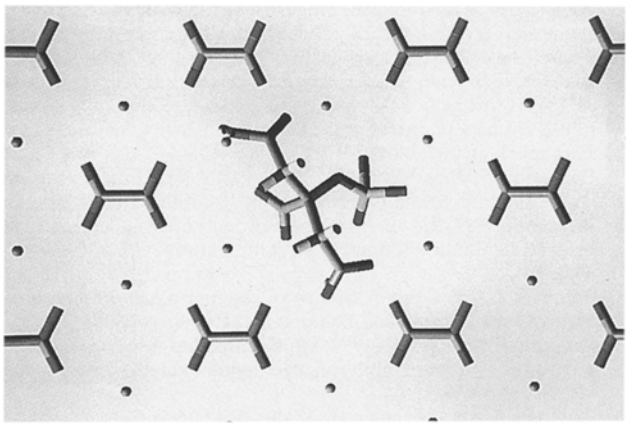

Fig. 10. Computer model of a PC molecule interacting with incomplete (−1 0 1) surface of COM. The molecule is coordinated more strongly with six calcium ions than in Figure 8, with three oxygens of the PO_4 group positioned into the surface. The hydrogen on the top α carboxyl is pointing away from the plane of the figure.

Acknowledgments. We are grateful for support from Research Corporation Grant C-3662, NSF Grant EHR-9108761, and an ARC Grant from the University of Tasmania. We also thank Todd Martin for computational assistance.

References

1. Richardson CF, Johnsson M, Bangash FK, Sharma VK, Sallis JD, Nancollas GH (1990) The effects of citrate and phosphocitrate on the kinetics of mineralization of calcium oxalate monohydrate. Mat Res Soc Symp Proc 174:87–92
2. Sallis JD, Brown MR, Parker NM (1991) Phosphorylated and nonphosphorylated carboxylic acids, influence of group substitution and comparison of compounds to phosphocitrate with respect to inhibition of calcium salt crystallization. In: Sikes CS, Wheeler AP (eds) ACS symposium series—surface reactive peptides and polymers. American Chemical Society Publishers, Washington, 149–160
3. Tiselius H-G, Berg C, Fornander A-M, Nilsson M-A (1993) Effects of citrate on the different phases of calcium oxalate crystallization. Scanning Microsc 7:381–390
4. Arnott HJ (1982) Three systems of biomineralization in plants with comments on the associated organic matrix. In: Nancollas GH (ed) Biological mineralization and demineralization. Springer-Verlag, New York, pp 199–218
5. Simkiss K, Wilbur KM (1989) Biomineralization, cell biology and mineral deposition. Academic Press Inc, New York
6. Lowenstam HA (1986) Mineralization processes in monerans and protoctists. Syst Assoc Spec 30:345–360
7. Wierzbicki A, Sikes CS, Madura JD, Drake B (1994) Atomic force microscopy and molecular modeling of protein and peptide binding to calcite. Calcif Tissue Int 54:133–141
8. Berman A, Addadi L, Weiner S (1988) Interactions of sea-urchin skeleton macromolecules with growing calcite crystals—a study of intercrystalline proteins. Nature 331:546–548
9. Moradian-Oldak J, Frolow F, Addadi L, Weiner S (1992) Interactions between acidic matrix macromolecules and calcium phosphate ester crystals: relevance to carbonate apatite formation in biomineralization. Proc R Soc Lond B 247:47–55
10. Mann S, Didymus JM, Sanderson NP, Heywood BH, Samper

EJA (1990) Morphological influence of functionalized and non-functionalized α,ω-dicarboxylates on calcite crystallization. J Chem Soc Faraday Trans 86:1873–1880
11. Black SN, Bromley LA, Cottier D, Davey RJ, Dobbs B, Rout JE (1991) Interactions at the organic/inorganic interface: binding motifs for phosphonates at the surface of barite crystals. J Chem Faraday Trans 87:3409–3414
12. Deganello S, Piro OE (1981) The crystal structure of calcium oxalate monohydrate (whewellite) N Jb Miner 2:81–88
13. Deganello S (1991) Interaction between nephrocalcin and calcium oxalate monohydrate: a structural study. Calcif Tissue Int 48:421–428
14. Sutor DJ (1969) Growth studies of calcium oxalate in the presence of various ions and compounds. B J Urol 41:171–178
15. Sallis JD, Lumley MF (1979) On the possible role of glycosaminoglycans as natural inhibitors of calcium oxalate stones. Invest Urol 16:296–299
16. Pankowski AH, Meehan JD, Sallis JD (1994) Synthesis via a cyclic dioxatrichloro-phosphorane of 1,3-dibenzyl-2-phosphonoxy citrate. Tetrahedron Lett 35:927–930
17. Madura JD, Wierzbicki A, Harrington JP, Maughon RH, Raymond JA, Sikes CS (1994) Interactions of the D- and L-forms of winter flounder antifreeze peptide with the [201] planes of ice. JACS 116:417–418
18. Tazzoli V, Domeneghetti C (1980) The crystal structures of whewellite and weddellite: re-examination and comparison. Am Mineral 65:3027–334
19. Glusker JP (1980) Citrate conformation and chelation: enzymatic implications. Acc Chem Res 13:345–352
20. Chirlian LE, Francl MM (1987) Atomic charges derived from electrostatic potentials: a detailed study. J Computational Chem 8:894–905
21. Breneman CM, Wiberg KB (1990) Determining atom-centered monopoles from molecular electrostatic potentials: the need for high sampling density in formamide conformational analysis. J Computational Chem 11:361–373
22. Dewar MJS, Thiel W (1977) Ground states of molecules 38. The MNDO method: approximations and parameters. JACS 99: 4899–4906
23. Hirst DM (1990) A computational approach to chemistry. Blackwell Scientific, Boston
24. Hehre WJ, Radom L, Schleyer VR, Pople JA (1986) *Ab initio* molecular orbital theory. Wiley and Sons, New York
25. Stout GH, Jensen LH (1989) X-ray structure determination: a practical guide. Wiley and Sons, New York
26. Main P, Fiske SJ, Hull SE, Lessinger L, Germain G, Declercq J-P, Woolfson WM (1980) MULTAN80. A system of computer programs for the automatic solution of crystal structures from x-ray diffraction data. University of York, England and Louvain, Belgium
27. International tables for x-ray crystallography, vol IV (1974) Kynoch Press, Birmingham, UK
28. Frenz BA (1982) SDP. The Enraf-Nonius CAD-4 structure determination program—a real-time system for concurrent x-ray data collection and crystal structure solution. In: Schenk H, Oltholf-Hazekamp R, van Koningsveld H, Bassi GC (eds) Computing in crystallography. Delft University Press, Delft, The Netherlands